

Hydrogen in layered iron arsenide: indirect electron doping to induce superconductivity

Taku Hanna,¹ Yoshinori Muraba,¹ Satoru Matsuishi,¹ Naoki Igawa,² Katsuaki Kodama,²
Shin-ichi Shamoto² and Hideo Hosono^{1,3,*}

¹*Materials and Structures Laboratory, Tokyo Institute of Technology, 4259 Nagatsuta-cho, Midori-ku, Yokohama 226-8503, Japan*

²*Quantum Beam Science Directorate, Japan Atomic Energy Agency, Tokai, Ibaraki 319-1195, Japan.*

³*Frontier Research Center, Tokyo Institute of Technology, 4259 Nagatsuta-cho, Midori-ku, Yokohama 226-8503, Japan*

Utilizing the high stability of calcium and rare earth hydrides, $\text{CaFeAsF}_{1-x}\text{H}_x$ ($x = 0.0-1.0$) and $\text{SmFeAsO}_{1-x}\text{H}_x$ ($x = 0.0-0.4$) have been synthesized using high pressure to form hydrogen-substituted 1111 type iron-arsenide superconductors. Neutron diffraction and density functional calculations have demonstrated that the hydrogens are incorporated as H^- ions occupying F^- sites in the blocking layer of CaFeAsF . The resulting $\text{CaFeAsF}_{1-x}\text{H}_x$ is non-superconducting, whereas $\text{SmFeAsO}_{1-x}\text{H}_x$ is superconductor, with an optimal $T_c = 55$ K at $x \sim 0.2$. It was found that up to 40% of the O^{2-} ions can be replaced by H^- ions, with electrons being supplied into the FeAs-layer to maintain neutrality ($\text{O}^{2-} = \text{H}^- + e^-$). When x exceeded 0.2, T_c was reduced corresponding to an electron over-doped region, which has not been previously seen.

PACS: 74.70.Xa, 74.62.Bf, 74.25.F-

*Corresponding author: Hideo Hosono

Materials and Structures Laboratory, Tokyo Institute of Technology

4259 Nagatsuta, Midori, Yokohama 226-8503, Japan

TEL +81-45-924-5359

FAX +81-45-924-5339

E-mail: hosono@msl.titech.ac.jp

Since the discovery of superconductivity in $\text{LaFeAsO}_{1-x}\text{F}_x$ ($T_c = 28$ K),¹ layered iron pnictides and related materials have been intensively investigated as candidates for high- T_c superconductors. To date, various types of iron-based superconductors have been synthesized²⁻¹¹, with the highest T_c of ~ 55 K being recorded in $\text{SmFeAsO}_{0.9}\text{F}_{0.1}$.¹²⁻¹⁷ The 1111 type iron arsenides LnFeAsO with a ZrCuSiAs -type structure¹⁸ are composed of stacks of alternating FeAs anti-fluorite-type conducting layers and LnO fluorite-type blocking layers. Although the parent compounds are non-superconducting at ambient pressures, they are superconducting when electrons are doped into the FeAs-layer via fluorine substitution at the oxygen sites ($\text{O}^{2-} = \text{F}^- + e^-$),^{1,13-17} oxygen vacancy formation ($\text{O}^{2-} = \text{V}_\text{O} + 2e^-$),¹⁹⁻²¹ or transition metal (a TM with excess electrons when compared with Fe, like Co or Ni) substitution into the iron site.²²⁻²⁵ TM -substitution, adding electrons to the FeAs-layer, is a “direct” doping mode, whereas F-substitution or O-vacancy formation is an “indirect” mode, because impurities are doped to the blocking layers and the electrons generated migrate to the FeAs layers. The general consensus is that indirect doping gives a higher T_c , because less structural and electrical disturbances occur in the superconducting layers. However, over-doping via the indirect mode has not been confirmed for most 1111 type iron-arsenides. In other words, further improvement in the T_c may be possible. For example, the solubility limit of fluorine substitution in LnFeAsO is lower than 20%. This is in contrast to alkali metal substitution in 122 type $\text{Ba}_{1-x}\text{K}_x\text{Fe}_2\text{As}_2$ superconductors, in which the Ba site can be fully replaced by K.²⁶ This restraint also makes it difficult to complete the electronic phase diagram (doping level vs. critical temperatures) beyond the optimal doping level. Completion of the phase diagram is important, not only to improve T_c , but also to understand superconductivity. Besides, although several papers have reported on the variation of T_c with nominal oxygen vacancy or hydrogen content in the 1111 system, the chemical states and the analyzed composition have not been clarified to date.^{19,20,27-29} This is an obstacle to understanding the emerging and carrier concentration dependence on T_c .

In this paper, we propose a novel method for indirect electron doping to induce superconductivity in 1111 type iron arsenides. By using a high pressure synthesis method with an excess hydrogen source, CaFeAsH has been synthesized, a new analog of LnFeAsO , and the solid solution between CaFeAsF ^{30,31} and CaFeAsH ($\text{CaFeAsF}_{1-x}\text{H}_x$ where $0 < x \leq 1$). While $\text{CaFeAsF}_{1-x}\text{H}_x$ is non-superconducting like LnFeAsO , these results indicate the anion site of blocking layer can be substituted by H^- . Considering the facile formation of metal hydrides with rare earths, H^- appears to be stabilized in these rare earth compounds. Thus, the hydrogen substitution technique has been applied to electron doping in SmFeAsO as with fluorine substitution ($\text{O}^{2-} = \text{F}^- + e^-$). Up to 40 % of the oxygen sites were successfully replaced by hydrogen ($\text{SmFeAsO}_{1-x}\text{H}_x$, $0 < x \leq 0.4$) and superconductivity with a maximum $T_c = 55$ K ($x \sim 0.2$) was induced. Above 20% hydrogen substitution, T_c was decreased, indicating that electron over-doping, which was not seen with F substitution in this system, was observed.³²⁻³⁴

CaFeAsH was synthesized by the solid state reaction of CaAs, Fe₂As and CaH₂ with LiAlH₄ as an excess hydrogen source, at 1000°C and 2 GPa (CaAs + Fe₂As + CaH₂ → 2CaFeAsH). A belt-type anvil cell was employed for the high pressure synthesis. Powders of CaAs and Fe₂As were prepared from their respective metals (Ca: 99.99% Aldrich, Fe: 99.9% Kojyundo, As: 99.9999% Kojyundo) and CaH₂/CaD₂ were synthesized by heating calcium metal in a H₂/D₂ atmosphere. All starting materials and precursors for the synthesis were prepared in a glove-box (Miwa Mfg.) filled with purified Ar gas (H₂O, O₂ < 1 ppm). The mixture of starting materials was placed into a BN capsule. Following the internal hydrogen source technique developed by Fukai and Okuma,^{35,36} LiAlH₄ (98%, Tokyo Kasei) was also placed in the capsule, with a BN separator, as a supplementary hydrogen source. The deuterated analog, CaFeAsD, was also prepared using CaD₂ and LiAlD₄ (98%, Aldrich). The resulting crystalline phases were identified by powder X-ray diffraction (XRD). Crystalline phases in the resulting samples were identified by powder X-ray diffraction (XRD) using a Bruker diffractometer model D8 ADVANCE (Cu rotating anode). The Rietveld analysis of XRD patterns was performed using TOPAS code.³⁷ Figure 1(a) shows powder XRD patterns of the resulting products at room temperature (RT). Except for several minor peaks due to Fe and Ca(OH₂)/Ca(OD₂) phases (< 5 wt.%), all the peaks were indexed to a tetragonal ZrCuSiAs type¹⁸ structure (space group: *P*/4*nmm*) with lattice constants *a* = 0.3878 nm and *c* = 0.8260 nm for CaFeAsH and *a* = 0.3876 nm and *c* = 0.8257 nm for CaFeAsD. The differences in the lattice constants between the hydride and deuteride versions were less than 0.05 %. Rietveld analysis indicated that the observed XRD pattern is well explained by assuming a model structure composed of alternate layers of FeAs and CaH(D). However the site position and occupancy of hydrogen cannot be determined by XRD, because the X-ray atomic scattering factor of H⁻/D⁻ is too small.

The amount of hydrogen incorporated in the resulting samples was evaluated by thermogravimetry/mass spectroscopy (TG-MS) performed using a Bruker AXS TG-DTA/MS9610 equipped with a gas feed port to inject the standard H₂ gas into the sample chamber. 20 mg of sample was heated up to 800 °C with a heating rate of 20 K·min⁻¹ under a helium gas flow. Hydrogen released from sample, in the form of H₂ molecule was ionized and detected by a quadrupole mass spectrometer as an ion with *m/z* = 2. As shown in Fig. 1 (b), weight loss involving the emission of H₂ molecule was observed from 200 to 600°C. The TG-MS measurement continued to 800°C, where the sample decomposed into a mixture of CaFe₂As₂, FeAs and unknown phases probably consisting of Ca with O₂, N₂ and/or H₂O gas from the He gas flow. The amount of released H₂ was estimated to be 3.08 mmol/g from the integration of the mass peak *m/z* = 2. This was almost equal to that expected for the decomposition of CaFeAsH (2CaFeAsH → Ca + CaFe₂As₂ + H₂↑, 2.91 mmol/g).

Since the coherent neutron scattering cross section of deuterium (5.592 barn) is comparable to that of Ca (2.78), Fe (11.22) or As (5.44),³⁸ the atomic position and site occupancy of deuterium can be determined by neutron powder diffraction (NPD). Neutron powder diffraction of CaFeAsD was measured on 3 grams of sample by the high resolution powder diffractometer (HRPD) installed at the

JRR-3 reactor of JAEA (beam collimation of 30'-40'-(sample)-6' with neutron wavelength $\lambda = 0.182391$ nm). Figure 1(c) shows NPD patterns observed at RT and 10 K. Rietveld analyses performed using RIETAN-FP code³⁹ revealed that the anion site in the block layer is occupied by deuterium, with the site occupancy of 0.935. Taking in to account the isotopic purity of the LiAlD₄ (98 %) and inclusion of hydrogen from other starting materials, we conclude that the remaining fraction (0.065) of the anion site is primarily occupied by hydrogen. The NPD pattern observed at 10 K was attributed to an orthorhombic phase, space group: *Cmma*, $a = 0.549213(16)$ nm, $b = 0.545660(16)$ nm, $c = 0.821154(24)$ nm. This crystal symmetry change is the same as in other 1111 type iron arsenides (*LnFeAsO* and *AeFeAsF*) with tetragonal to orthorhombic transitions reported in the range of 120-180 K. High pressure synthesis appears to be essential for the formation of CaFeAsH, because no such phase has been prepared at ambient pressures.

Figure 2 (a) shows the temperature dependence of dc electrical resistivity (ρ) in CaFeAsH and CaFeAsD measured from 300 to 2 K, using a physical properties measurements system (PPMS, Quantum Design). Both samples exhibit sudden decreases at ~ 100 K (T_{anom}). This anomaly has also been observed in 1111 and 122 type iron arsenides and has been attributed to a tetragonal to orthorhombic transition.

Figure 2 (b) shows the calculated total and projected density of states (DOS and PDOS) of CaFeAsH obtained by density functional calculations using density functional theory (DFT), the generalized gradient approximation functional PBE,⁴⁰ and the projected augmented waves method⁴² implemented in the Vienna ab initio simulation program (VASP) code,⁴² following refs. ^{43,44} and 50. A $\sqrt{2}a \times \sqrt{2}b \times 2c$ supercell containing 8 chemical formulae was used for the calculation and the plane-wave basis set cutoff was set to 600 eV. For Brillouin zone integrations to calculate the total energy and DOS, $4 \times 4 \times 2$ Monkhorst-Pack grids of k -points were used. The total energy was minimized with respect to both the coordinates of all atoms and lattice parameters. Then, the stripe type anti-ferromagnetic ordering of the Fe spins, commonly observed for 1111 type Fe arsenides below T_{anom} , was obtained as the most stable magnetic structure. To obtain the projected DOS, the charge density was decomposed over the atom-centered spherical harmonics with Wigner-Seitz radius $r = (3V_{\text{cell}}/4\pi N)^{1/3}$, where V_{cell} and N are the unit cell volume and the number of atoms in an unit cell, respectively. Total DOS and Fe PDOS profiles revealed the semi-metallic nature of CaFeAsH, with Fe 3d up-spin and down-spin bands overlapped at the Fermi level ($E = 0$). Hydrogen 1s levels were located ~ 2 eV below the Fermi level and were fully occupied. It is evident from these results that hydrogen is incorporated as H^- ($1s^2$) in CaFeAsH. This finding is consistent with the similarities in the ρ - T curves of CaFeAsH and CaFeAsF, indicating that the replacement of F sites with H^- ions does not seriously affect the electronic structure of the FeAs conduction layer.

Based on the similarity of the charge and size of the hydride and fluorine ion, the formation of the solid solution $\text{CaFeAsF}_{1-x}\text{H}_x$ was expected, and was obtained over the full x range by adding CaF_2 to the starting mixture in the high pressure synthesis, $\text{CaAs} + \text{Fe}_2\text{As} + (1-x) \text{CaF}_2 + x \text{CaH}_2 \rightarrow 2\text{CaFeAsF}_{1-x}\text{H}_x$. Figure 2 (c) shows the lattice parameters a and c as a function of x . The value of x

in the resulting $\text{CaFeAsF}_{1-x}\text{H}_x$ was evaluated by TG-MS measurement. While the lattice parameter a was almost independent of x , the value of c was proportional to x , indicating that the geometry of the $\text{CaF}_{1-x}\text{H}_x$ layer is determined by the weighted average of the ionic radius of F^- (r_{F}) and H^- (r_{H}). From the F-Ca distance ($r_{\text{F}} + r_{\text{Ca}} = 233.7 \text{ pm}$)⁴⁵ and the H-Ca bond length ($r_{\text{H}} + r_{\text{Ca}} = 230.2 \text{ pm}$) evaluated from the Rietveld analysis, the ionic radius of H^- was estimated for 1111 type iron-arsenides. On the assumption that a F^- coordinated by four Ca^{2+} ions retains Shanon's ionic radius ($r_{\text{F}} = 131 \text{ pm}$),³⁴ then the ionic radius of Ca^{2+} was calculated to be 102.7 pm. The radius of H^- calculated from the H-Ca bond length (230.2 pm) in CaFeAsH is 127.5 pm, which is smaller than that of F^- by 2.8%. Chevalier et al.⁴⁶⁻⁴⁸ reported the synthesis of 1111 type hydrides LnMXH (Ln = lanthanides; M = Mn, Fe and Co; X = Si and Ge). These were composed of stacks of alternating LnH hydride layers and MX layers made by hydrogen insertion to CeFsSi -type⁴⁹ LnMX . In contrast, the present high pressure synthesis using hydrides does not require the precursor.

Next, the hydrogen substitution technique was applied to electron doping in SmFeAsO . Like $\text{CaFeAsF}_{1-x}\text{H}_x$, $\text{SmFeAsO}_{1-x}\text{H}_x$ was prepared by the solid state reaction of SmAs , FeAs , Fe_2As , Sm_2O_3 and SmH_2 at 2 GPa at 1200 °C; $(2+x) \text{ SmAs} + (2+x) \text{ Fe}_2\text{As} + (2-2x) \text{ FeAs} + (2-2x) \text{ Sm}_2\text{O}_3 + 3x \text{ SmH}_2 \rightarrow 6\text{SmFeAsO}_{1-x}\text{H}_x$. SmAs and SmH_2 were prepared by the reaction of Sm metal with arsenic or hydrogen gas. In this case, a mixture of NaBH_4 and $\text{Ca}(\text{OH})_2$ was used as the excess hydrogen source. Figure 3 (a) shows representative powder XRD patterns of $\text{SmFeAsO}_{1-x}\text{H}_x$ (nominal x values in starting mixtures are 0.1, 0.3 and 0.5). When nominal x exceeds ~ 0.4 , the SmAs phase begins to segregate, implying the actual hydrogen content (x) is lower than the nominal x . Figure 3(b) shows TG-MS profile ($m/z = 2$) of $\text{SmFeAsO}_{1-x}\text{H}_x$ with nominal $x = 0.15$. Hydrogen incorporated in $\text{SmFeAsO}_{1-x}\text{H}_x$ was released between 400 and 800°C. The line shape of the emission curve is close to that of $\text{CaFeAsF}_{1-x}\text{H}_x$. Figure 3 (c) compares hydrogen (x) and oxygen contents (y) in prepared samples per chemical formula ($\text{SmFeAsO}_y\text{H}_x$), as a function of nominal x in the starting mixture. The former value was determined by TG-MS and the latter was measured with a JEOL JXA-8530F electron-probe micro-analyzer (EPMA) equipped with a field emission-type electron gun and wavelength dispersive X-ray (WDX) detectors. The micro scale compositions within the main phase were probed on 5-10 focal points and the results were averaged. For nominal $x \leq 0.4$, the hydrogen content agrees with the nominal x and the deficient amount of oxygen ($1 - y$), indicating the oxygen site (O^{2-}) was successfully substituted with hydrogen (H^-). Figure 3 (d) shows the variation of lattice constants a and c of $\text{SmFeAsO}_{1-x}\text{H}_x$ system. Same as $\text{CaFeAsF}_{1-x}\text{H}_x$, the decrease of c with x corresponds the difference in ionic radii between O^{2-} (142 pm) and H^- (127.5 pm in $\text{CaFeAsF}_{1-x}\text{H}_x$). On the other hand, a of the $\text{SmFeAsO}_{1-x}\text{H}_x$ system apparently decreases with x . This result contrasts with the $\text{CaFeAsF}_{1-x}\text{H}_x$ system, in which a is independent of x . It is likely to be a result of electron doping in the FeAs layer by H substitution ($\text{O}^{2-} = \text{H}^- + \text{e}^-$), i.e., the doped electrons occupy the bonding states of FeAs layer, and shorten the intra-layer Fe-Fe distance.

Figure 4(a) shows the temperature dependence of the electrical resistivity in $\text{SmFeAsO}_{1-x}\text{H}_x$.

A sudden drop of resistivity due to superconductivity was observed for $x \geq 0.03$ and the maximum critical temperature T_c (onset) was 55 K at $x \sim 0.2$. As x increased over 0.2, T_c decreased, indicating the appearance of an over-doped region. Figure 4 (b) shows x - T diagram of $\text{SmFeAsO}_{1-x}\text{H}_x$ superimposed with that of $\text{SmFeAsO}_{1-x}\text{F}_x$ with the fluorine content x measured by EPMA as reported by A. Köhler et al.³³ T_c vs. x plots of $\text{SmFeAsO}_{1-x}\text{H}_x$ and $\text{SmFeAsO}_{1-x}\text{F}_x$ overlap at $x < 0.15$, indicating that hydrogen gives indirect electron doping to the FeAs-layer just like fluorine. While the solubility limit of fluorine in the oxygen site is restricted to less than 20 % ($x = 0.2$),^{33,34} hydrogen can reach 40 %. The wider substitution range is useful for the optimization of the electron doping level to induce superconductivity and to complete the electronic phase diagram, including the over-doped region. The sample of $x = 0.03$ shows both the sudden drop of resistivity due to superconducting transition ($T_c = 5$ K) and the ρ - T anomaly ($T_{\text{anorm}} = 114$ K) due to crystallographic transition accompanied with magnetic ordering of the Fe spins. Similar behavior has been observed in $\text{SmFeAsO}_{1-x}\text{F}_x$ around $x \sim 0.04$.³² These results imply the coexistence of superconductivity and magnetic ordering in the limited x range near 0.03-0.04. While such coexistence has been confirmed in 122 type iron arsenide superconductors,²⁶ it is hard to distinguish the coexistence in systems with compositional disorder. Detailed experiments using an appropriate microprobe such as μSR are required to clarify the intrinsic nature of this coexistence.

In summary, 1111 type $\text{CaFeAsF}_{1-x}\text{H}_x$ ($0 < x \leq 1$) and $\text{SmFeAsO}_{1-x}\text{H}_x$ ($0 < x \leq 0.4$) were successfully synthesized by a high pressure technique with an excess hydrogen source. Substitution of H^- into the F^- site in CaFeAsF was confirmed by neutron powder diffraction analysis and density functional calculations. The resulting $\text{CaFeAsF}_{1-x}\text{H}_x$ were non-superconducting, with a ρ - T anomaly at ~ 100 K due to a tetragonal to orthorhombic transition commonly observed in AeFeAsF and LnFeAsO . In $\text{SmFeAsO}_{1-x}\text{H}_x$ ($0 < x \leq 0.4$), H^- substitution into the O^{2-} site supplies electrons to the FeAs-layer, giving raise to superconductivity with an optimized T_c of 55 K. Further H^- -substitution beyond the optimal level leads to a decrease in T_c up to $x = 0.4$. The present results suggest the hydrogen (H^-) substitution to the anion site is generally applicable for electron doping in 1111 type iron-arsenide superconductors.

We thank Drs. Toshiyuki Atou and Osamu Fukunaga of Tokyo Institute of Technology for their valuable discussions. This study was supported by the Funding Program for World-Leading Innovative R&D on Science and Technology, JSPS, Japan.

- ¹ Y. Kamihara, T. Watanabe, M. Hirano, and H. Hosono, *Journal of the American Chemical Society* **130**, 3296-3297 (2008).
- ² M. Rotter, M. Tegel, and D. Johrendt, *Phys. Rev. Lett.* **101**, 107006 (2008).
- ³ C. Gen-Fu, L. Zheng, L. Gang, H. Wan-Zheng, D. Jing, Z. Jun, Z. Xiao-Dong, Z. Ping, W. Nan-Lin, and L. Jian-Lin, *Chinese Phys. Lett.* **25**, 3403-3405 (2008).
- ⁴ G. Wu, H. Chen, T. Wu, Y.L. Xie, Y.J. Yan, R.H. Liu, X.F. Wang, J.J. Ying, and X.H. Chen, *J. Phys.: Condens. Matter* **20**, 422201 (2008).
- ⁵ F. Hsu, J. Luo, K. Yeh, T. Chen, T. Huang, P.M. Wu, Y. Lee, Y. Huang, Y. Chu, D. Yan, and M. Wu, *Proceedings of the National Academy of Sciences* **105**, 14262 -14264 (2008).
- ⁶ X. Wang, Q. Liu, Y. Lv, W. Gao, L. Yang, R. Yu, F. Li, and C. Jin, *Solid State Communications* **148**, 538-540 (2008).
- ⁷ H. Ogino, Y. Matsumura, Y. Katsura, K. Ushiyama, S. Horii, K. Kishio, and J. Shimoyama, *Supercond. Sci. Technol.* **22**, 075008 (2009).
- ⁸ X. Zhu, F. Han, G. Mu, P. Cheng, B. Shen, B. Zeng, and H. Wen, *Sci. China Ser. G-Phys. Mech. Astron.* **52**, 1876-1878 (2010).
- ⁹ X. Zhu, F. Han, G. Mu, P. Cheng, B. Shen, B. Zeng, and H. H. Wen, *Phys. Rev. B* **79**, 220512 (2009).
- ¹⁰ G.F. Chen, T. Xia, H.X. Yang, J.Q. Li, P. Zheng, J.L. Luo, and N.L. Wang, *Supercond. Sci. Technol.* **22**, 072001 (2009).
- ¹¹ J. Guo, S. Jin, G. Wang, S. Wang, K. Zhu, T. Zhou, M. He, and X. Chen, *Phys. Rev. B* **82**, 180520 (2010).
- ¹² H. Takahashi, K. Igawa, K. Arii, Y. Kamihara, M. Hirano, and H. Hosono, *Nature* **453**, 376-378 (2008).
- ¹³ G.F. Chen, Z. Li, D. Wu, G. Li, W.Z. Hu, J. Dong, P. Zheng, J.L. Luo, and N.L. Wang, *Phys. Rev. Lett.* **100**, 247002 (2008).
- ¹⁴ Z.A. Ren, J. Yang, W. Lu, W. Yi, G.C. Che, X.L. Dong, L.L. Sun, and Z.X. Zhao, *Materials Research Innovations* **12**, 105-106 (2008).
- ¹⁵ Z. Ren, J. Yang, W. Lu, W. Yi, X. Shen, Z. Li, G. Che, X. Dong, L. Sun, F. Zhou, and Z. Zhao, *Europhys. Lett.* **82**, 57002 (2008).
- ¹⁶ X.H. Chen, T. Wu, G. Wu, R.H. Liu, H. Chen, and D.F. Fang, *Nature* **453**, 761-762 (2008).
- ¹⁷ R. Zhi-An, L. Wei, Y. Jie, Y. Wei, S. Xiao-Li, Zheng-Cai, C. Guang-Can, D. Xiao-Li, S. Li-Ling, Z. Fang, and Z. Zhong-Xian, *Chinese Phys. Lett.* **25**, 2215-2216 (2008).
- ¹⁸ R. Pottgen and D. Johrendt, *Zeitschrift Für Naturforschung* **63b**, 1135 (2008).
- ¹⁹ Z. Ren, G. Che, X. Dong, J. Yang, W. Lu, W. Yi, X. Shen, Z. Li, L. Sun, F. Zhou, and Z. Zhao, *Europhys. Lett.* **83**, 17002 (2008).
- ²⁰ H. Kito, H. Eisaki, and A. Iyo, *J. Phys. Soc. Jpn.* **77**, 063707 (2008).
- ²¹ K. Miyazawa, K. Kihou, P.M. Shirage, C. Lee, H. Kito, H. Eisaki, and A. Iyo, *J. Phys. Soc. Jpn.* **78**, 034712 (2009).
- ²² A.S. Sefat, A. Huq, M.A. McGuire, R. Jin, B.C. Sales, D. Mandrus, L.M.D. Cranswick, P.W. Stephens, and K.H. Stone, *Phys. Rev. B* **78**, 104505 (2008).
- ²³ C. Wang, Y.K. Li, Z.W. Zhu, S. Jiang, X. Lin, Y.K. Luo, S. Chi, L.J. Li, Z. Ren, M. He, H. Chen, Y.T. Wang, Q. Tao, G.H. Cao, and Z.A. Xu, *Phys. Rev. B* **79**, 054521 (2009).
- ²⁴ G. Cao, S. Jiang, X. Lin, C. Wang, Y. Li, Z. Ren, Q. Tao, C. Feng, J. Dai, Z. Xu, and F. C. Zhang, *Phys. Rev. B* **79**, 174505 (2009).
- ²⁵ Y.K. Li, X. Lin, T. Zhou, J.Q. Shen, Q. Tao, G.H. Cao, and Z.A. Xu, *J. Phys.: Condens. Matter* **21**, 355702 (2009).
- ²⁶ H. Chen, Y. Ren, Y. Qiu, W. Bao, R.H. Liu, G. Wu, T. Wu, Y.L. Xie, X.F. Wang, Q. Huang, and X.H. Chen, *Epl* **85**, 5 (2009).
- ²⁷ K. Miyazawa, K. Kihou, P.M. Shirage, C. Lee, H. Kito, H. Eisaki, and A. Iyo, *J. Phys. Soc. Jpn.* **78**, 034712 (2009).

- ²⁸ P.M. Shirage, K. Miyazawa, K. Kihou, H. Kito, Y. Yoshida, Y. Tanaka, H. Eisaki, and A. Iyo, *Phys. Rev. Lett.* **105**, 037004 (2010).
- ²⁹ K. Miyazawa, S. Ishida, K. Kihou, P.M. Shirage, M. Nakajima, C.H. Lee, H. Kito, Y. Tomioka, T. Ito, H. Eisaki, H. Yamashita, H. Mukuda, K. Tokiwa, S. Uchida, and A. Iyo, *Appl. Phys. Lett.* **96**, 072514 (2010).
- ³⁰ S. Matsuishi, Y. Inoue, T. Nomura, H. Yanagi, M. Hirano, and H. Hosono, *Journal of the American Chemical Society* **130**, 14428-14429 (2008).
- ³¹ S. Matsuishi, Y. Inoue, T. Nomura, Y. Kamihara, M. Hirano, and H. Hosono, *New J. Phys.* **11**, 025012 (2009).
- ³² Y. Kamihara, T. Nomura, M. Hirano, J. Eun Kim, K. Kato, M. Takata, Y. Kobayashi, S. Kitao, S. Higashitaniguchi, Y. Yoda, M. Seto, and H. Hosono, *New J. Phys.* **12**, 033005 (2010).
- ³³ A. Köhler and G. Behr, *J Supercond Nov Magn* **22**, 565-567 (2009).
- ³⁴ G. Prando, P. Carretta, A. Rigamonti, S. Sanna, A. Palenzona, M. Putti, and M. Tropeano, *Phys. Rev. B* **81**, 100508 (2010).
- ³⁵ Y. Fukai and N. Okuma, *Jpn. J. Appl. Phys.* **32**, L1256-L1259 (1993).
- ³⁶ Y. Fukai and N. Okuma, *Phys. Rev. Lett.* **73**, 1640 (1994).
- ³⁷ Bruker AXS, (2009).
- ³⁸ V.F. Sears, *Neutron News* **3**, 26-37 (1992).
- ³⁹ F. Izumi and K. Momma, *Ssp* **130**, 15-20 (2007).
- ⁴⁰ J.P. Perdew, K. Burke, and M. Ernzerhof, *Phys. Rev. Lett.* **77**, 3865 (1996); **78**, 1396(E) (1997).
- ⁴¹ P.E. Blöchl, *Phys. Rev. B* **50**, 17953 (1994).
- ⁴² G. Kresse and J. Furthmüller, *Phys. Rev. B* **54**, 11169 (1996).
- ⁴³ T. Nomura, S.W. Kim, Y. Kamihara, M. Hirano, P.V. Sushko, K. Kato, M. Takata, A.L. Shluger, and H. Hosono, *Supercond. Sci. Technol.* **21**, 125028 (2008).
- ⁴⁴ P.V. Sushko, A.L. Shluger, M. Hirano, and H. Hosono, *Phys. Rev. B* **78**, 172508 (2008).
- ⁴⁵ R.D. Shannon, *Acta Cryst A* **32**, 751-767 (1976).
- ⁴⁶ B. Chevalier and S.F. Matar, *Phys. Rev. B* **70**, 174408 (2004).
- ⁴⁷ B. Chevalier, E. Gaudin, S. Tencé, B. Malaman, J.R. Fernandez, G. André, and B. Coqblin, *Phys. Rev. B* **77**, 014414 (2008).
- ⁴⁸ B. Chevalier, M. Pasturel, J. Bobet, and O. Isnard, *Solid State Communications* **134**, 529-533 (2005).
- ⁴⁹ O.I. Bodak, E.I. Gladyshevskii, and P.I. Kripyakevich, *J Struct Chem* **11**, 283-288 (1970).

Figure captions

Fig.1 (a) Powder XRD patterns of CaFeAsH and CaFeAsD at room temperature. (b) TG and MS ($m/z = 2$ corresponds to the H₂ molecule) profiles of CaFeAsH. Weight loss due the decomposition of sample with hydrogen emission was observed from 200 to 600°C. Hydrogen concentration was estimated to be 1.05 molecules per unit cell by integration of the MS trace curve. (c) Neutron powder diffraction pattern of CaFeAsD observed at 300 K and 10 K (d) Crystal structure of CaFeAsD(H). (e) Crystal structure of CaFeAsH at 300 K (tetragonal) and 10 K (orthorhombic)

Fig.2 (a) ρ - T profile of CaFeAsH and CaFeAsD compared with CaFeAsF. (b) Total and atomic projected density of states of CaFeAsH obtained by density functional calculation using VASP code. The origin was set to the Fermi Level. (c) Variation of lattice constants (a , c) as function of x in the solid solution CaFeAsF_{1-x}H_x. Hydrogen content (x) was estimated by TG-MS method.

Fig.3 (a) Powder XRD patterns of SmFeAsO_{1-x}H_x (nominal $x = 0.3, 0.4$ and 0.5). Insets show close up views. (b) TG and MS ($m/z = 2$) profiles of SmFeAsO_{1-x}H_x with nominal $x = 0.15$. H₂ gas emission associated with weight loss was observed from 400 to 800°C. (c) Oxygen content determined by EPMA measurement (y) and hydrogen content estimated by TG-MS method (x) in SmFeAsO_yH_x as a function of nominal x in starting mixture. Total anion content ($x + y$) is almost equal to unity, indicating the deficiency of oxygen site is wholly compensated by hydrogen. (d) Lattice constants (a and c) of SmFeAsO_{1-x}H_x as a function of x .

Fig.4 (a) ρ - T profiles of SmFeAsO_{1-x}H_x in under-doped (left; $x = 0.0$ - 0.19) and over-doped states (right; $x = 0.22$ - 0.47). (b) x - T diagram of SmFeAsO_{1-x}H_x superimposed by that of SmFeAsO_{1-x}F_x.³³

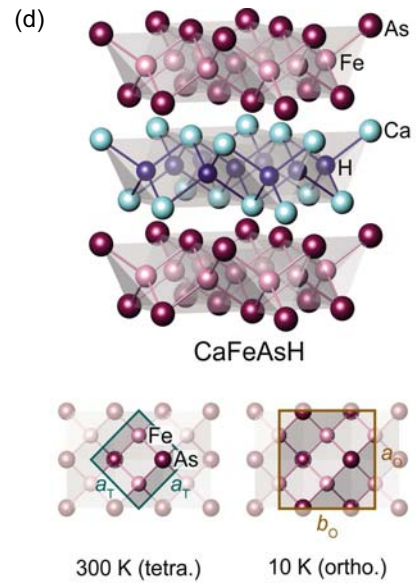
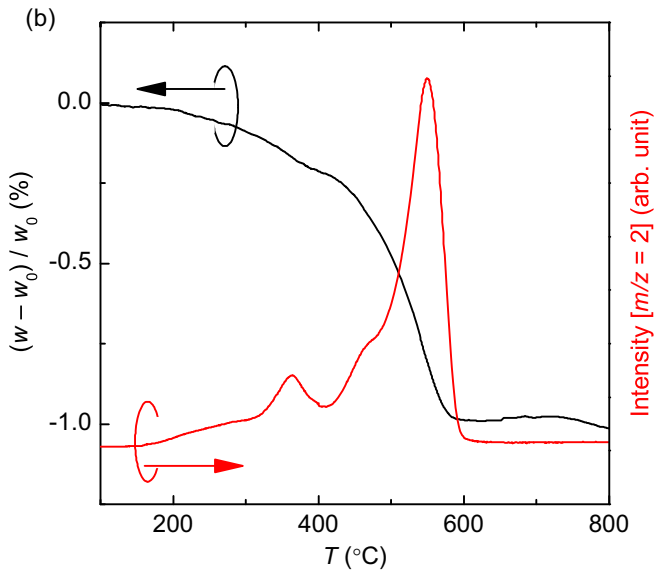
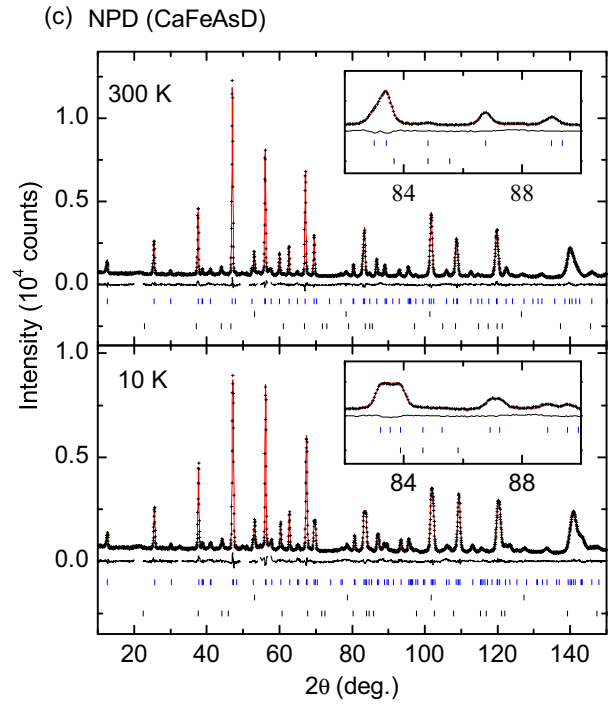
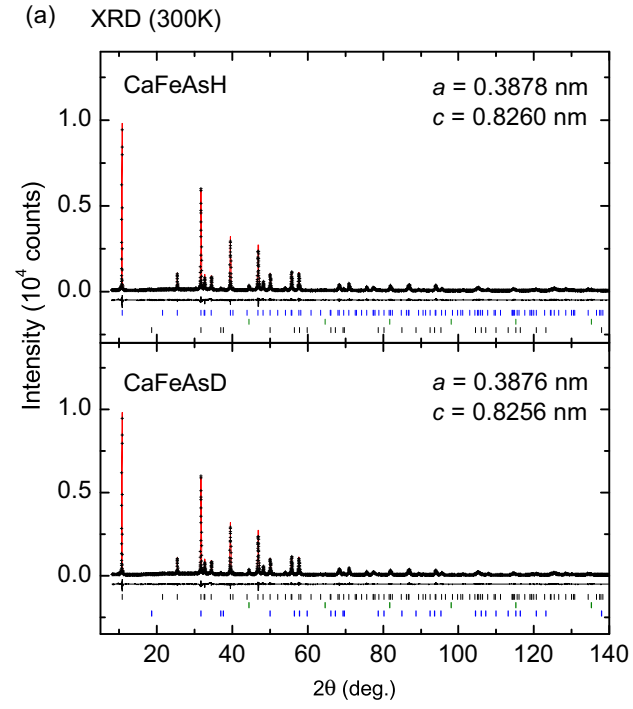


Fig.1

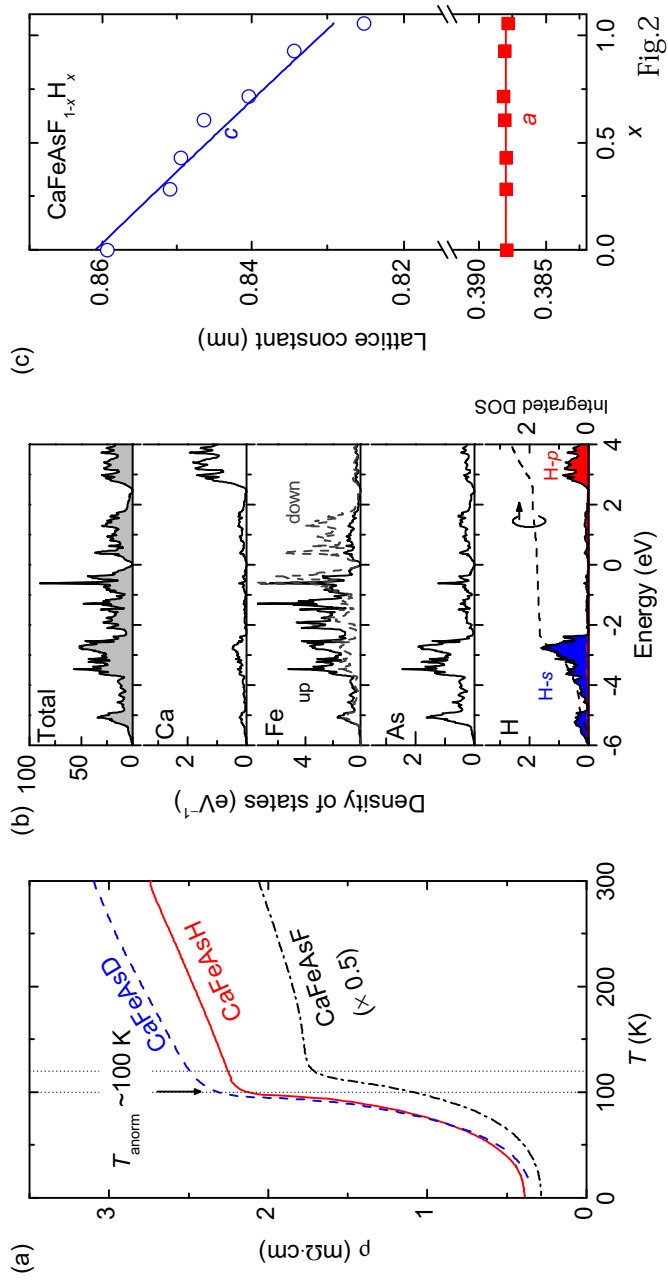


Fig.2

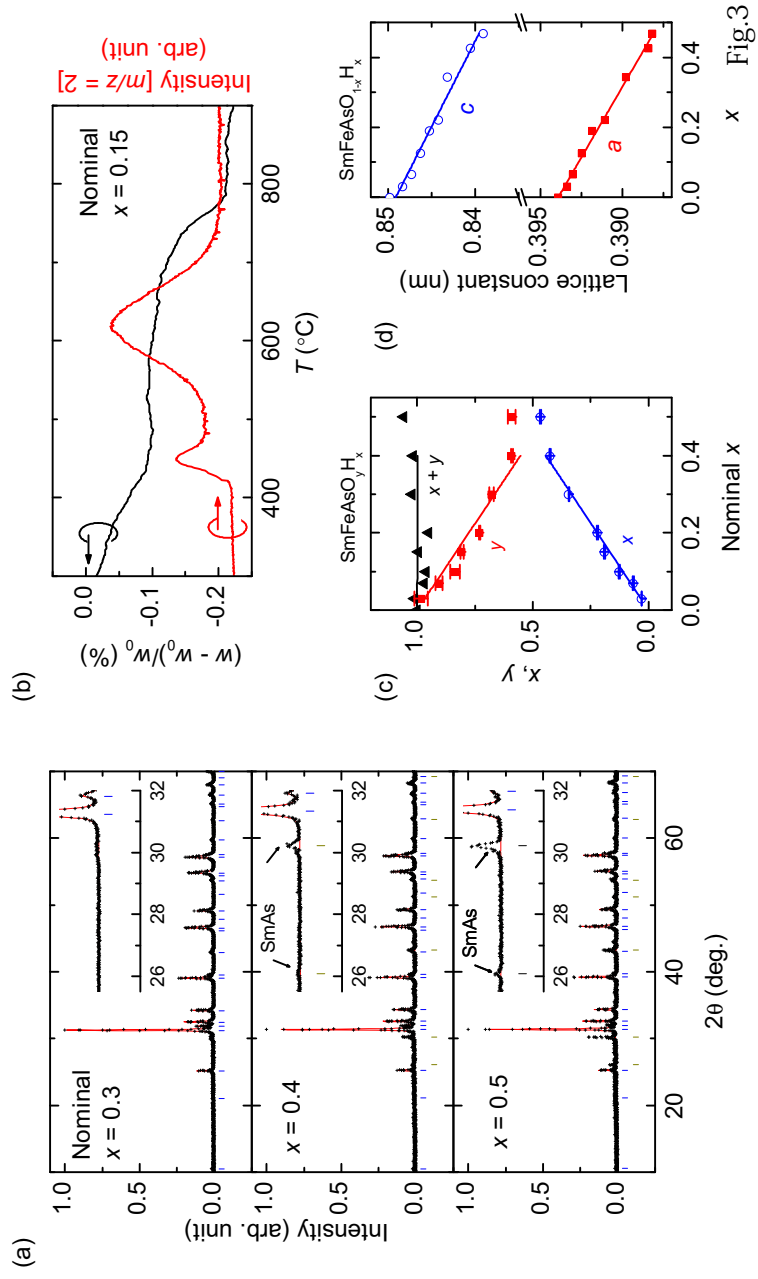


Fig.3

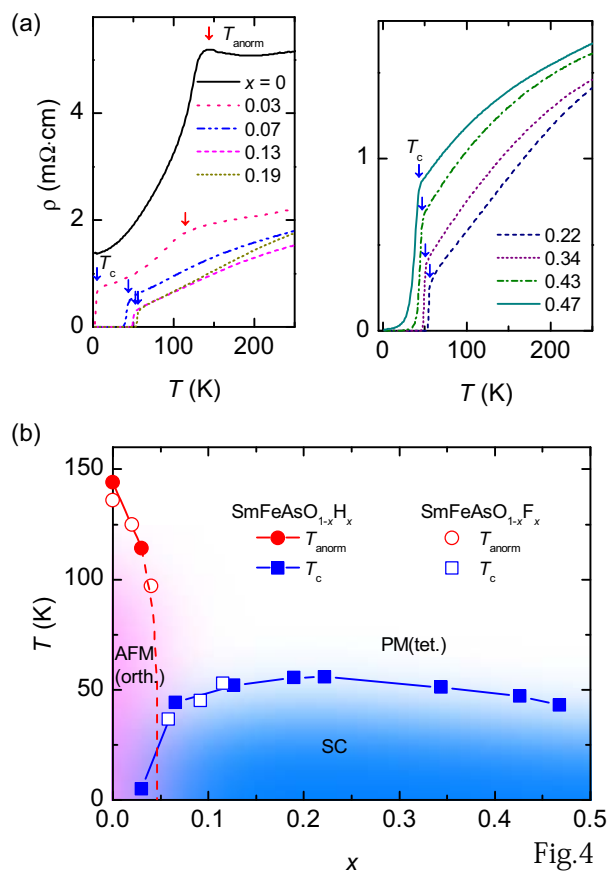


Fig.4